RESEARCH PAPER

Evolution of nano-pores in illite-dominant clay during consolidation

Yanhao Zheng[1,2] · Béatrice A. Baudet[2] (ORCID)

Abstract

In this paper, the evolution of nanoscale pores, covering inter-particle pores and inter-layer pores, in illite-dominant clay during consolidation is monitored using small angle X-ray scattering (SAXS) and nitrogen gas adsorption (N_2GA) techniques. No obvious change observed in the characteristic peaks of SAXS intensity curves during consolidation suggests that the intra-particle structure of the clay, including interlayer spacings, is not affected by mechanical loading, at least up to 4 MPa. The N_2GA test results show that the volume of inter-particle pores inside the aggregates does decrease gradually as the compression proceeds, which is accompanied by a gradual reduction in specific surface area, probably due to the rearrangement of the particles composing the aggregates. The inter-particle pores are compressed as a whole during consolidation instead of the progressive collapse in an ordered manner, from the larger to the smaller. By comparing the pore-size distributions of illite-dominant clay obtained by MIP (mercury intrusion porosimetry) and N_2GA techniques, it is found that the shapes of the two distributions in the common measurement range are obviously not matched, essentially due to the sequential nature of the drying and wetting processes. While filling the research gap in the evolution of intra-aggregate pores during consolidation, this study also shows that the N_2GA technique and SAXS measurement used in conjunction with each other appear as a powerful approach for clay nano-pores identification.

Keywords Consolidation · Inter-layer pores · Inter-particle pores · Nitrogen gas adsorption · Small-angle X-ray scattering

Abbreviations

e	Global void ratio
d	Interplanar crystal spacing of the crystal lattice
D	Entrance pore diameter
I	X-ray intensity
θ	Scattering angle
P	Absolute equilibrium pressure
P_0	Condensation pressure of nitrogen in laboratory conditions
q	Scattering vector
λ	Wavelength of the incident X-ray beam
1D	One-dimensional
BET	Brunauer–Emmett–Tellers
BJH	Barrett–Joyner–Halenda
BSCS	British Soil Classification System
BSI	British Standards Institution
DSC	Differential scanning calorimetry
IUPAC	International Union of Pure and Applied Chemistry
MIP	Mercury intrusion porosimetry
N_2GA	Nitrogen gas adsorption
PSD	Pore size distribution
SAXS	Small angle X-ray scattering
SSA	Specific surface area
STP	Standard temperature and pressure
TGA	Thermogravimetric analysis

✉ Yanhao Zheng
  yanhao.zheng.18@ucl.ac.uk

1 School of Civil and Environmental Engineering, Harbin Institute of Technology (Shenzhen), Shenzhen, China

2 Department of Civil, Environmental and Geomatic Engineering, University College London, London, UK

1 Introduction

For a clay normally consolidated to a given effective stress, clay particles, made up of unit clay layers (elementary silicate sheets) stacking face to face, group together to form aggregates, and the random arrangement of aggregates forms clay fabric [3]. Within this microstructure, pore populations are generally classified into three categories: (1) inter-layer pores, which are the planar interlayer spaces between the unit clay layers inside the clay particles; (2)

inter-particle pores, which are the small voids between the clay particles within the aggregates; (3) inter-aggregate pores, which are the large voids between the assembly of aggregates. Many studies have suggested that the collapse of inter-aggregate pores is responsible for the macroscopic volume change during consolidation and that the mechanical compression has no effect on the inter-particle pores and inter-layer pores (both collectively known as intra-aggregate pores) [13, 15, 32, 42]. This was based on the fact that the pore size distribution curves at different consolidation pressures, measured by mercury intrusion porosimetry (MIP) technique, nearly coincided at the nanoscale.

To intrude small empty pores, which may correspond to intra-aggregate pores, mercury has to be forced by pressures that are thought to be high enough to reopen some closed pores or affect the size of intra-aggregate pores to some extent [16]. The counter-argument is that the soil's pore system should already be mostly filled with incompressible mercury when reaching the point of needing higher pressures, and therefore, the pore structure should be able to withstand such high pressures without compressing [13, 36, 40]. This theory stands unchallenged when considering the structure of inter-aggregate pores, as large pores should have already been filled up at low pressures. For the smaller pores that are not yet filled and may be inaccessible, such as inter-particle and inter-layer pores, the high mercury pressures still have the potential to break the pore structure of these small pores, though their pore volumes are very small and have little effect on the overall MIP results. One known limitation of the MIP technique however is that mercury pressures generally cannot go higher than 210 MPa, i.e., pores with entry diameters smaller than 5 nm, such as the interlayer spacing inside the particles, cannot be reached. While such data on the intra-aggregate porosity are rare [13, 19], they have become relevant for modellers who rely on the pore size distribution to assess engineering properties of fine-grained soils or develop discrete element models for clays. This paper provides experimental data on nanoscale pores during compression, using non-invasive techniques other than MIP and which can monitor the evolution of inter-particle pores and inter-layer pores.

Nitrogen gas adsorption (N_2GA) is a common method to detect small pores and it has been widely used to characterize the pore size distribution and porosity of materials such as clays [4, 25, 33, 35], mudstones and shales [11, 25, 45], and other nanoporous materials such as microporous carbons [27, 31]. Relying on Brunauer–Emmett–Tellers (BET) multilayer adsorption theory [9], this technique is also often employed to determine the specific surface area (SSA) of the soil [25, 35, 38]. Another method uses methylene blue adsorption, and a study by

Hegyesi et al. [23], which compared the SSA measured by BET theory and methylene blue adsorption method, showed that the specific surface area determined by N_2GA was comparatively small because of the limited amount of nitrogen molecules that can penetrate into interlayer vacancies of the silicates. This was also found by Santamarina et al. [38], who demonstrated that most nitrogen molecules could only reach the external surface of the clay particle. For this reason, the interlayer spacing inside clay particles is often evaluated using a supplementary technique: small-angle X-ray scattering (SAXS) [5, 26, 30]. In the present work, both SAXS and N_2GA tests were conducted on an illite-dominant clay consolidated to different maximum stresses. The measured data from the SAXS and N_2GA tests were used to monitor the evolution of inter-layer pores and inter-particle pores, respectively, during consolidation.

2 Materials and sample preparations

The soil investigated in this study was obtained by separating the fines fraction of an illite-rich parent clayey loess from Jingyang, China, from the coarser particles by sedimentation. The soil tested had lost its initial structure and was no longer collapsible. The index properties of the soil were measured in the laboratory following BSI 1377-2:1990, as summarized in Table 1. According to the

Table 1 Geotechnical characteristics of the soil

	Measured value
Specific gravity	2.73
Atterberg limits	
Liquid limit (%)	55.5
Plastic limit (%)	20.1
Plasticity index	35.4
Grain size distribution	
Percentage of sand (0.06–2.0 mm) (%)	0
Percentage of silt (0.002–0.06 mm) (%)	50.2
Percentage of clay (< 0.002 mm) (%)	49.8
Mineralogical compositions	
Quartz (%)	10.4
Albite (%)	5.2
Biotite (%)	1.1
Calcite (%)	16.5
Montmorillonite (%)	8.6
Illite (%)	48.2
Kaolinite (%)	5.5
Chlorite (%)	4.4

British Soil Classification System (BSCS), this soil is classified as a clay with high plasticity. The mineralogical composition was identified quantitatively using a PANalytical X'Pert Pro diffractometer (see Table 1), showing that the clay mineral of the soil is 66.7% with a dominant presence of illite (48.2%), followed by nearly 10% independent montmorillonite, and half of the remaining 34.3% non-clay minerals are calcite (16.5%).

The samples were prepared to be in a reconstituted state by mixing the soil with deionized water at a water content of 1.25 times the liquid limit, as suggested by [7]. The uniform clay slurries were firstly vacuumed to remove trapped air bubbles and then one-dimensionally consolidated by standard oedometer tests in accordance with BSI 1377-5:1990, with an approximate 1.5 load increment ratio, to different maximum vertical effective stresses of 100, 400, 1000 and 2000 kPa. Each loading lasted for at least 24 h or until the end of primary consolidation. After reaching equilibrium at the desired loading stage, as much water as possible in the oedometer cell was removed, and then the clay was unloaded as quickly as possible, which ensured undrained unloading conditions, restraining swelling thanks to the build-up of an internal suction [41]. After removing the clay sample from the oedometer cell quickly, the excess water attached to the sample was wiped off before measurement. Then, the consolidated samples were wrapped in cling film and wax in a quick manner and then stored in a highly humid environmental chamber for the micro-analysis tests. This method has been widely applied in the microstructure analysis of clay and has been proven to be very effective in preserving the clay microstructure [21, 22, 47]. In practice, by using this method, the void ratio of clay samples measured after the oedometer test is also found to be almost the same as that measured before the microscopic test, with an error of less than 0.01. Therefore, the pore structure of the clay sample taken out from the oedometer cell can therefore be considered to represent that of the clay sample consolidated to the desired stress level.

The oedometer compression and swelling curves are shown in Fig. 1, where the compression index is 0.394 and the swelling index is 0.067. The initial void ratio of each odometer test was strictly controlled with an accuracy of $\pm$ 0.02 by using the methods proposed by Rocchi and Coop [37]. Details of the tests and the accuracy of initial void ratio were described by Zheng et al. [47].

The saturated samples consolidated at different maximum stresses (shown as the circled points in Fig. 1) were trimmed into small cubic sticks with a thin wire, then quickly frozen using liquid nitrogen at $-220\ °C$, and finally placed in a vacuum chamber to sublimate for 24 h. In this way, the capillary effect was minimized and the clay microstructure was in the state of minimal disturbance [13].
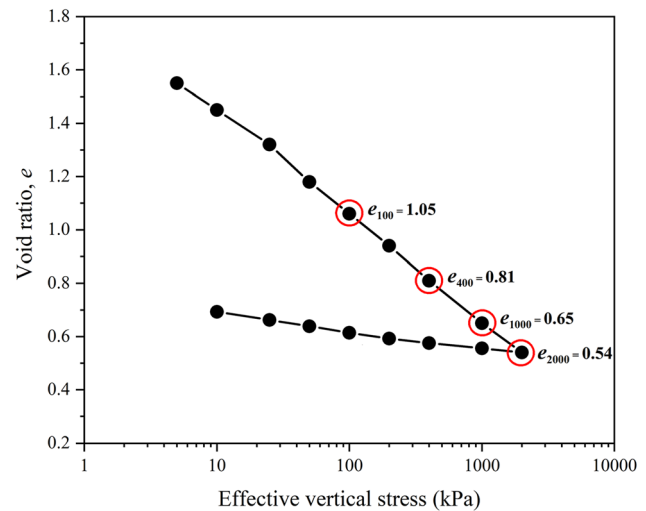

Fig. 1 Oedometer compression and swelling curves for the reconstituted illite-dominant clay (the points in the red circle are the states selected for nano-pore analysis)

This freeze-drying process is currently recognised as the most effective method for the removal of water from a clay mass without affecting soil microstructure, which has been largely adopted [12–14, 34, 44, 47]. The obtained dehydrated specimens were used for SAXS and N_2GA tests, each sample measuring around 3 mm long, 3 mm wide and 0.5 mm thick for SAXS measurements and around 5 mm long, 3 mm wide and 3 mm thick for N_2GA tests. Note that unlike usual SAXS and gas adsorption tests the clay samples were tested in a non-powder form. The thickness of the sample for SAXS measurement could not exceed 1 mm, otherwise the X-ray beam would not penetrate the sample.

3 Testing programme and methods

3.1 Small angle X-ray scattering (SAXS)

The SAXS measurements were performed using an Anton Paar SAXSpoint 2.0 instrument, operated at 40 kV and 50 mA with the automated scatterless beam collimation (fully evacuated). The microfocus X-ray source (Primux 100 micro) was employed to produce the CuKα radiation with a wavelength $\lambda = 0.1542$ nm. The freeze-dried samples were enclosed into the vacuum-tight quartz tube at room temperature. The sample-to-detector distance was 112.5 mm, resulting in the range of scattering vector (q) from about 0.5 to 20 nm^{-1}. The exposure time of each measurement was chosen as 30 min, as after 30 min, the change in peak intensity is no longer significant with the increase of exposure time. Intensity profiles were recorded with a two-dimensional imaging plate and the corresponding scattering intensities were measured via

SAXSdrive^{TM} software (Anton Paar) to generate two-dimensional data sets. The two-dimensional intensity data were then converted to one-dimensional scattering curves of the magnitude of the scattering vector, q-value, against intensity $I(q)$, offering the nano-structural information of the samples.

At the particle level, the fundamental structural element that composes the clay particle is the unit clay layer formed by one or two silica tetrahedral sheets and one alumina octahedral sheet (1:1 layer or 2:1 layer). The unit clay layers are stacked randomly in the third dimension to form different clay mineral crystals [2]. In the SAXS measurement, the interlayer spacing within clay mineral crystals can be characterized by the distance between layers of scatterers (d) [5]. Based on Bragg's law (Eq. 1) [20], the interplanar crystal spacing (d) is related to the scattering vector (q) and the scattering angle (2θ):

$$d = \lambda/2sin\theta = 2\pi/q \qquad (1)$$

where λ is the wavelength of the incident X-ray beam noted above. The characteristic spacings between adjacent clay layers inside the clay particles, i.e., d-values, can be extracted from the peak positions in the one-dimensional scattering curve based on the corresponding characteristic scattering vectors (q). The evolution of d-values during consolidation can thus be monitored directly by shifts or broadening of the initial peaks that are related to the uniform or non-uniform strain of particles [5].

3.2 Nitrogen gas adsorption (N₂GA)

The N₂GA tests were conducted using a Micromeritics ASAP 2020 HD88 Analyzer. Normally, the soil sample should be degassed at a proper temperature for at least 12 h in a vacuum oven. The main purpose of degassing is to ensure that any bound and capillary water adsorbed with the clay is completely removed so that the nitrogen gas can be adsorbed normally and completely on the surfaces, reducing any risk of damage to the apparatus and optimising the accuracy of the measurements [24]. In this study, since the clay samples had been freeze-dried before the degassing process, the free water and clay-bound water within the soil had been completely removed while keeping the soil microstructure intact [12, 13, 47]. Therefore, no water evaporation should have occurred during the degassing process, nor any shrinkage or distortion of pores [43]. But as an extra safety measure, the freeze-dried samples were still degassed at 200 °C in a vacuum oven filled with helium for about 2 h. It should be emphasized that within the measurement range of the N₂GA test, there was no significant change in the pore structure of the freeze-dried samples before and after degassing, which had been verified in practice by N₂GA testing and SEM observations.

The degassing temperature of 200 °C was determined by simultaneous thermogravimetric (TGA) and differential scanning calorimetry (DSC) analyses on the as-received illite-dominant clay powder with a TA SDT Q600 simultaneous thermal analyzer, as the excessive temperature can lead to irreversible changes in soil structure (such as surface colour changes). Results of the thermogravimetric examination (TGA and DSC curves) by heating the 5–10 mg of clay powder at the constant heating rate of 5 °C/min over the temperature range of 25–1100 °C under the flow of high purity argon (100 cm^3/min) are given in Fig. 2. In the DSC curve, the first endotherm peak occurs at 170.4 °C, indicative of the removal of the free water, weakly and strongly bound water in the illite clay because substances other than water have thermal stability at this temperature. The second endotherm peak is at 667.2 °C, probable due to the dehydroxylation of clay minerals near this temperature, partly breaking the structure of the crystalline lattice. Therefore, a value of 200 °C was chosen for this illite-dominant clay, between the temperature needed for the removal of the free water and clay-bound water (170.4 °C) and that for the dehydroxylation of clay minerals (667.2 °C). Then, the degassed samples were exposed to ultra-high purity 5.0 grade nitrogen gas at standard 77 K (liquid nitrogen temperature), and the nitrogen was adsorbed at different controlled pressures. The adsorption and desorption isotherms were finally obtained to determine the specific surface area and quantify the size distribution of pores between 2 and 150 nm.

The Brunauer–Emmett–Tellers (BET) multilayer adsorption theory [9] was used to determine the specific surface area by inverting the adsorption isotherm at different relative pressures (P/P_0) of 0.05–0.30 [24], where P is the absolute equilibrium pressure and P_0 is the condensation pressure of nitrogen in laboratory conditions.
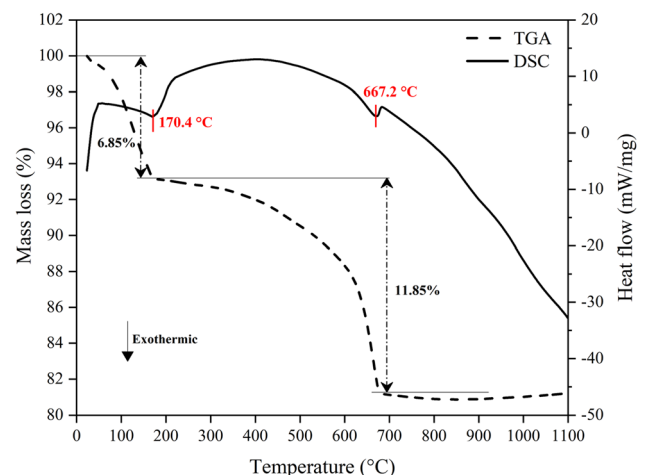

Fig. 2 TGA and DSC curves for the as-received illite-dominant clay powder heated from 25 to 1100 °C under high purity argon flow

The pore-size distribution was evaluated by Barrett–Joyner–Halenda (BJH) model based on the capillary condensation phenomenon in the pores [1]. The BJH method relates the pore diameter with the relative pressures (P/P_0) based on Kelvin's equation, assuming cylindrical and non-connecting pore geometry. The theoretical background of BET theory and BJH method were comprehensively elaborated by Gregg and Sing [18] and Kuila [24].

In addition to the SAXS and N_2GA tests, MIP tests were carried out on the oven-dried and freeze-dried soil samples, both of which were previously subjected to one-dimensional consolidation to two different stress levels, namely, 0 kPa and 1000 kPa, by using a Micromeritics AutoPore IV 9500 Automated Mercury Porosimeter. It is noted that only the MIP data in Sect. 4.4, used for comparing the pore-size distribution obtained from MIP and N2GA techniques, are reproduced from Zheng et al. [47]. Detailed testing procedures can be found in Zheng et al. [47]. A Hitachi HT7700 transmission electron microscope (TEM) and a JEOL JSM-6480LV scanning electron microscope (SEM) were finally used for observing the freeze-dried samples in slurry state (i.e., consolidation pressure is 0 kPa) in order to give a more intuitive view of the clay microstructure and the nano-pores inside the clay and inter-layer spacing.

4 Results and discussion

4.1 Identification of intra-aggregate pores

From SEM observation (Fig. 3), the slurry clay has a very loose and honeycomb-like microstructure. Overall, the structure can be considered as an aggregated microstructure, which is characterised by inter-aggregate pores (highlighted by yellow in ellipses) and intra-aggregate pores (highlighted by red in squares). The clay has a visibly flocculated structure when in slurry state, and the particle association in such a structure is edge-to-face and edge-to-edge flocculated and aggregated. No dispersed clay particles are observed in Fig. 3. The large pores between aggregates that are composed of the stacking of platelike clay particles can be up to 5 μm. While the size of intra-aggregate pores (highlighted in red), belonging to the nanoscale, is roughly less than 200 nm, which is compatible with the size of intra-aggregate pores in the existing literature [13, 19, 25, 44]. For clays such as that tested here, with clear aggregated microstructure in its initial state, the deformation responses during consolidation are controlled by aggregate-to-aggregate interactions rather than particle-to-particle interactions [13, 29, 44, 47].

Several studies have demonstrated that for saturated clay bodies, the high capillary forces established in the pores when water evaporates during oven-drying lead to a significant reduction in total porosity, corresponding to the very significant shrinkage of the clay sample at the macro level [13, 16, 42–44]. By comparing the pore-size distribution of oven-dried and freeze-dried soil samples, both Delage and Lefebvre [13] and Yu et al. [44] found that in the oven-drying process, the significant reduction in the volume of inter-aggregate pores is the main reason for this very extensive shrinkage, while the intra-aggregate porosity was barely affected, characterising oven-dried soil sample.

Based on this knowledge, Fig. 4 compares the pore size distribution of oven-dried and freeze-dried soil samples at two different stress levels, obtained by MIP tests. At the initial slurry state (consolidated at 0 kPa), the major peak of the freeze-dried sample is about 3 μm, which is consistent with the observation of the size of inter-aggregate pores in Fig. 3. After oven-drying, this major peak shifts to a small size of about 0.1 μm whereby the pores with a size of about 0.1 μm are considered to be the intra-aggregate pores, which is compatible with previous findings about illitic clays [13, 47]. The comparison of the pore-size distribution between oven-dried and freeze-dried soil samples at 0 kPa shows that the collapse of the inter-aggregate pores is mainly responsible for the significant shrinkage caused by oven drying. For this illite-dominant clay with a stable aggregate structure, the oven-drying process transforms the larger inter-aggregate pores into smaller intra-aggregate pores, which leads to a noticeable increase in the volume of intra-aggregate pores, and the intra-aggregate porosity is overwhelmingly dominant in the oven-dried clay sample, which is consistent with the findings by Delage and Lefebvre [13] on Champlain sensitive illitic clay and by Yu et al. [44] on the Speswhite kaolin. It is also interesting to find that when the compression proceeded from 0 to 1000 kPa, the major pores of the oven-dried samples moved to the left on the graph from about 0.1 to 0.08 μm, similarly to what is observed on freeze-dried samples. As the oven-drying process has little effect on intra-aggregate porosity [13, 44], this shift can be interpreted as the intra-aggregate pores, smaller than 100 nm for this illite-dominant clay, being also affected by the loading.

The TEM images (Fig. 5a, b) give a more distinct view of intra- aggregate pores, i.e., inter-layer pores and inter-particle pores. Figure 5a shows a typical inter-particle pore, separated by walls made up of the stacking of unit clay layers. The varying thickness of the pore wall might be due to the stacking of different mineral layers or the stacking of different layers of the same mineral. Such inter-particle pore (in the white circle) is subcircular and has a size of around 30 nm. Figure 5b presents a clearer structure of the "wall" and the inter-layer pores are the distances
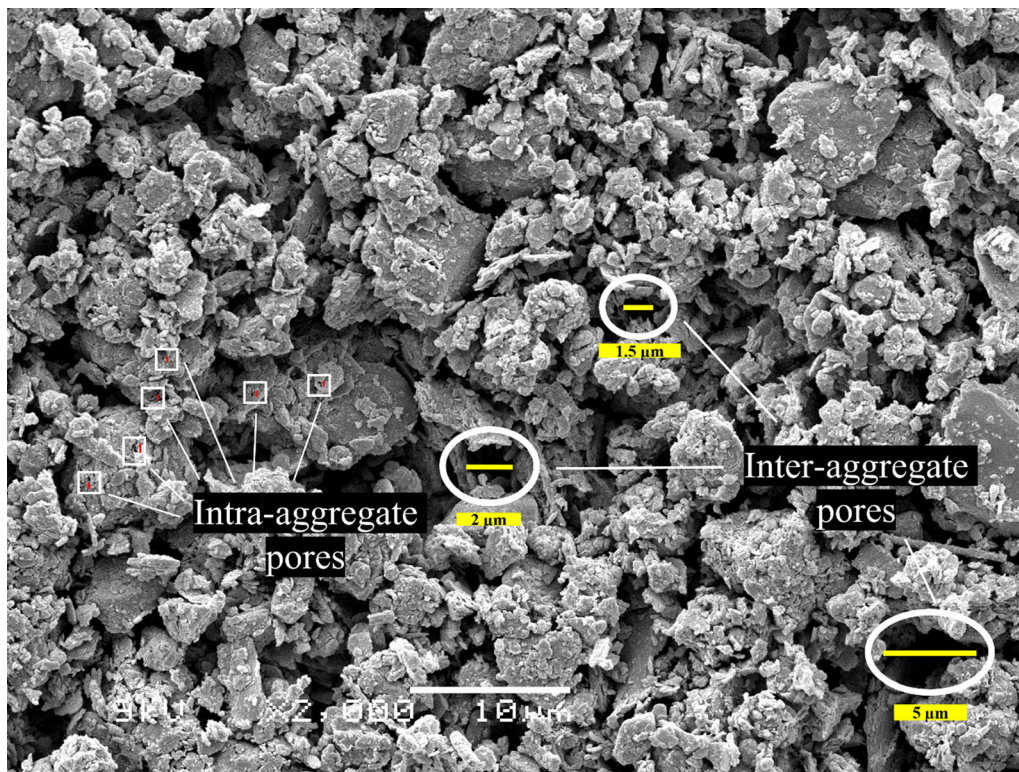
Fig. 3 SEM image of the freeze-dried clay sample in slurry state (consolidated at 0 kPa)
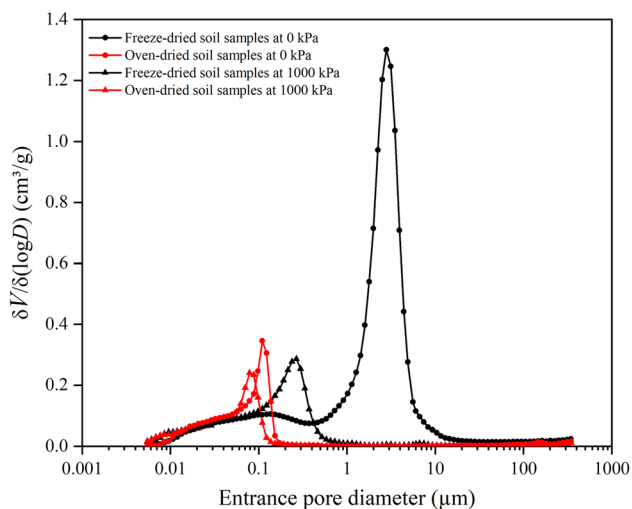

Fig. 4 Pore size distribution of the oven-dried and freeze-dried soil samples with the maximum consolidation pressure of 0 kPa and 1000 kPa

between the individual unit clay layers within the wall. Such a typical stack is 43.2 nm thick, which might be made up here of around 45 elementary illite layers stacked in a face-to-face arrangement, given that the inter-basal spacing of illite minerals is 0.96 nm [29], or of the stacking of around 20 montmorillonite layers with four adsorbed water layers because the soil is fully saturated, given that the

inter-basal spacing of the hydrated montmorillonite minerals in a 4W hydration state is 2.16 nm [14] and the tested soil contains 8.6% of montmorillonite (Table 1).

4.2 Inter-layer pores characterization

The inter-layer spacings inside the clay particles were characterized by SAXS technique. Several characteristic peaks are identified in the 1D SAXS scattering intensity curves (see Fig. 6), and these peaks correspond to the characteristic interplanar crystal spacings of different clay minerals. According to Eq. 1, the characteristic spacings between adjacent clay layers, i.e., d-values, were calculated. It should be noted that there is a set of different d-values for the same clay mineral, because clay minerals have multiple crystal faces and the d value represents the interplanar crystal spacing of the crystal lattice in a certain direction [8]. Referring to the Powder Diffraction File edited by the International Centre for Diffraction Data (ICDD), the d-values of 1.428 nm at $q = 4.40$ nm^{-1} and 0.450 nm at $q = 13.95$ nm^{-1} represent the montmorillonite minerals, $d_{(001)}$ and $d_{(110)}$, respectively; the d-value of 0.385 nm at $q = 16.21$ nm^{-1} represent the illite mineral, $d_{(11\bar{3})}$, and the d-values of 1.007 nm at $q = 6.24$ nm^{-1}, $d_{(002)}$, corresponds to the illite basal unit that composes the illite mineral; the d-values of 0.433 nm at $q = 14.68$ nm^{-1}
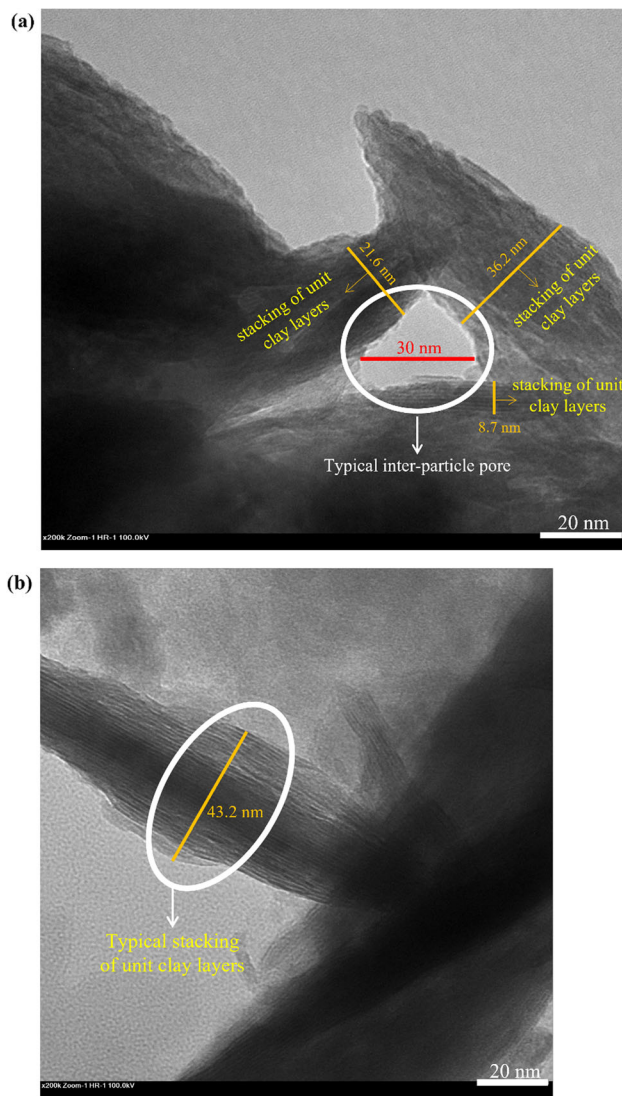
Fig. 5 a TEM photo of a typical inter-particle pore within the consolidated clay; and b TEM photo of a typical pore wall made up of the stacking of unit clay layers within the consolidated clay

and 0.336 nm at $q = 18.69$ nm^{-1} represent the kaolinite minerals, $d_{(1\bar{1}0)}$ and $d_{(111)}$, respectively; and the d-value of 0.711 nm at $q = 8.82$ nm^{-1} represents the chlorite mineral, $d_{(002)}$. The spacings between the neighbouring clay mineral layers are generally governed by hydrogen bonds, dipole–dipole interactions, or van der Waals forces between the octahedral sheet and the tetrahedral sheet of the adjacent layer [46].

Although it is generally accepted that mechanical loading has little effect on the intra-particle structure of clay minerals, there is little experimental evidence to support this view. Since Fig. 4 is indicated that the intra-aggregate porosity of this illite-dominant clay is also affected by the 1D compression loading, it is necessary to explore whether the inter-layer pores, as part of the intra-

aggregate pores, evolve during consolidation. The SAXS test results (Fig. 6) show that the positions and shapes of these characteristic peaks at different stress levels are almost unchanged, except for the downward movement of the scattering intensity with increasing consolidation pressure. The decrease in intensity is to be expected, because the intensity value indicates the number of scatterers inside the sample. Under a similar volume, the sample consolidated to a higher stress is denser than that consolidated to a lower stress, so a smaller number of scatterers pass through the sample with a higher consolidation pressure during the same exposure time. The absence of evolution of those characteristic peaks (the appearance of new peaks or the shifts of initial peaks) suggested no significant change in inter-layer pores occurred as the compression proceeded. Considering that the consolidation pressure of 2 MPa was still too small to compress the inter-layer pores, a supplementary SAXS test was carried out on the freeze-dried clay sample consolidated to 4 MPa, to further explore the effect of consolidation pressure on inter-layer pores. Still no obvious change observed in those characteristic peaks (see Fig. 6) demonstrated that the intra-particle structure of these clay minerals, including interlayer spacings (inter-layer pores), were not affected by 1D compression loading, at least up to 4 MPa, even when large strains are measured at the macro-scale. It is noted that the SAXS intensity curves become less smooth in the range of 6–14 nm^{-1} in the case that the consolidation pressure was 2000 kPa and 4000 kPa, which cannot be interpreted by the change in the number of inter-layer pores within this range. This phenomenon can be attributed to the fact that compared to clay samples consolidated at other lower stress levels, the samples with maximum consolidation pressures of 2000 kPa and 4000 kPa are denser and therefore a smaller number of scatterers would be able to pass through them over the same exposure time, resulting in the scatters received by the detector that were not very stable and coherent.

4.3 Inter-particle pores characterization

The inter-particle pores, arising from the uneven packing of the particles, with various sizes and thicknesses within the aggregates, were characterized by N$_2$GA tests. Assuming that the pore wall is uniformly covered by nitrogen, the specific surface area (SSA) of the soil was determined based on BET theory [9], as the volume of absorbed nitrogen is proportional to the soil's surface area (including external surface and pore surface) [25]. As shown in Table 2, the SSA sees a slight and gradual reduction with increasing vertical effective stress, from 55.47 m^2/g at 100 kPa to 54.07 m^2/g at 400 kPa, then 52.31 m^2/g at 1000 kPa, and finally to 51.38 m^2/g at 2000 kPa. This
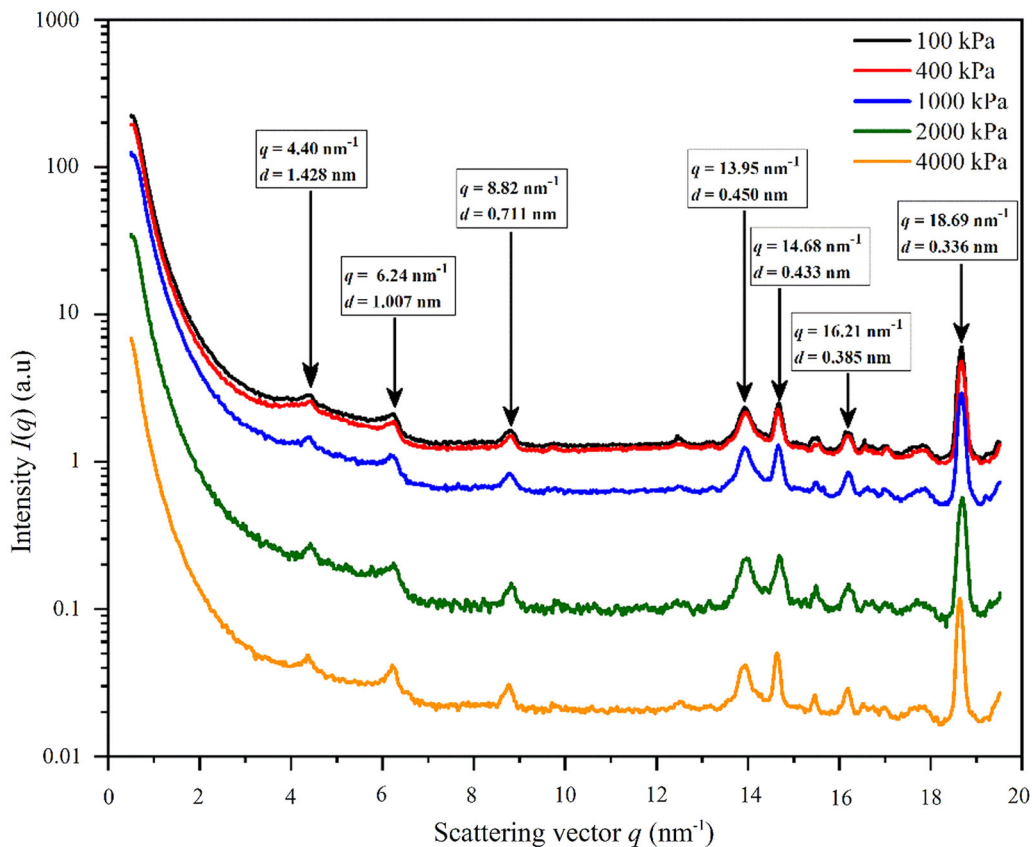
Fig. 6 1D SAXS intensity curves for the reconstituted illite-dominant clay with different maximum consolidation pressures

Table 2 Specific surface area of the clay at various consolidation pressures, obtained by the BET method

Vertical effective stress (kPa)	100 kPa	400 kPa	1000 kPa	2000 kPa
Specific surface area (m^2/g)	55.47	54.07	52.31	51.38

indicates that although the elongation of the pores induced by loading can increase the specific surface area to some extent, consolidation may have caused some pores to become smaller or even closed, due to the compaction of the aggregates, with the rearrangement of the particles composing them, explaining the gradual decrease of SSA.

Figure 7 shows the adsorption–desorption isotherms of the clay samples consolidated at different maximum stresses. Each isotherm is irreversible with a typical hysteresis loop. The shape and the hysteresis pattern of the isotherm provide useful information on the mechanism of the physical adsorption process, which can be used to qualitatively evaluate the types of pores present in the soil [25]. These isotherms have a similar shape with a sudden disappearance of the hysteresis at P/P_0 of 0.4. The only
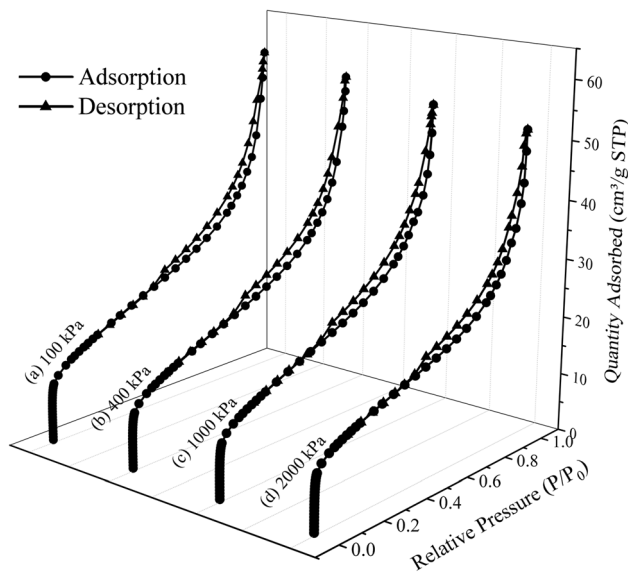

Fig. 7 Nitrogen adsorption–desorption isotherms of the reconstituted illite-dominant clay with different maximum consolidation pressures: **a** 100 kPa; **b** 400 kPa; **c** 1000 kPa; and **d** 2000 kPa, at standard temperature and pressure (STP) where the standard temperature is 273 K (0 °C or 32° Fahrenheit) and the standard pressure is 1 atm pressure

difference is that the nitrogen quantity adsorbed decreased slightly at P/P_0 of 1.0 with increasing consolidation pressure, corresponding to the gradual reduction of specific surface area. According to the isotherm classification group suggested by the International Union of Pure and Applied Chemistry (IUPAC), there are six types of gas adsorption–desorption isotherms (Type I–Type VI) and four types of hysteresis patterns (Type H_1–Type H_4) usually found in materials [39]. Such an isotherm shape has a close resemblance to the Type IV isotherm, but the plateau disappears at higher relative pressures (P/P_0 close to 1.0) instead of the volume uptake. The absence of the plateau and the steep slopes in the high relative pressure range ($0.98 < P/P_0 < 1.0$) suggest the existence of macropores (> 50 nm according to IUPAC classification), while the high adsorption volume at lower relative pressures ($P/P_0 < 0.1$) suggests the presence of micropores (< 2 nm, IUPAC) [25]. The Type H_3 hysteresis loop based on IUPAC classification suggests that most of the pores are slit-shaped [39], which corresponds to the shape of pores due to aggregation and consolidation.

The cumulative and density function pore size distribution (PSD) curves, as illustrated in Fig. 8, were derived from the adsorption branches of the nitrogen adsorption–desorption isotherms based on the BJH model. In Fig. 8a, as the stress increased, the cumulative pore volume gradually decreased by 0.015 cm^3/g, from 0.098 cm^3/g at 100 kPa to 0.083 cm^3/g at 2000 kPa, and the corresponding reduction in void ratio was 0.041, obtained by multiplying the decreased adsorbed pore volume (0.15 cm^3/g) by the particle density of the clay (2.73 g/cm^3). The reduction of 0.041 in the voids between particles was very small compared to that of 0.51 in global void ratio (from 1.05 at 100 to 0.64 at 2000 kPa in Fig. 1). Although this small reduction can be considered to have little effect on the macroscopic deformation of the clay during consolidation, it suggested that the inter-particle pores were also compressed gradually with increasing stress level, which is probably due to the rearrangement of the particles composing the aggregates.

The pore size density function curves in Fig. 8b are characterized by several peaks and these peaks do not shift with the load level. No global leftwards shift of the peaks indicates that the collapse of inter-particle pores under mechanical compression was not in an ordered manner, from the larger to the smaller, different from the pore collapse mechanism for inter-aggregate pores [13, 15]. In other words, the inter-particle pores within the aggregates were compressed as a whole during consolidation, rather than by the phenomenon that smaller inter-particle pores could not be compressed until the larger ones had been collapsed [13, 15].
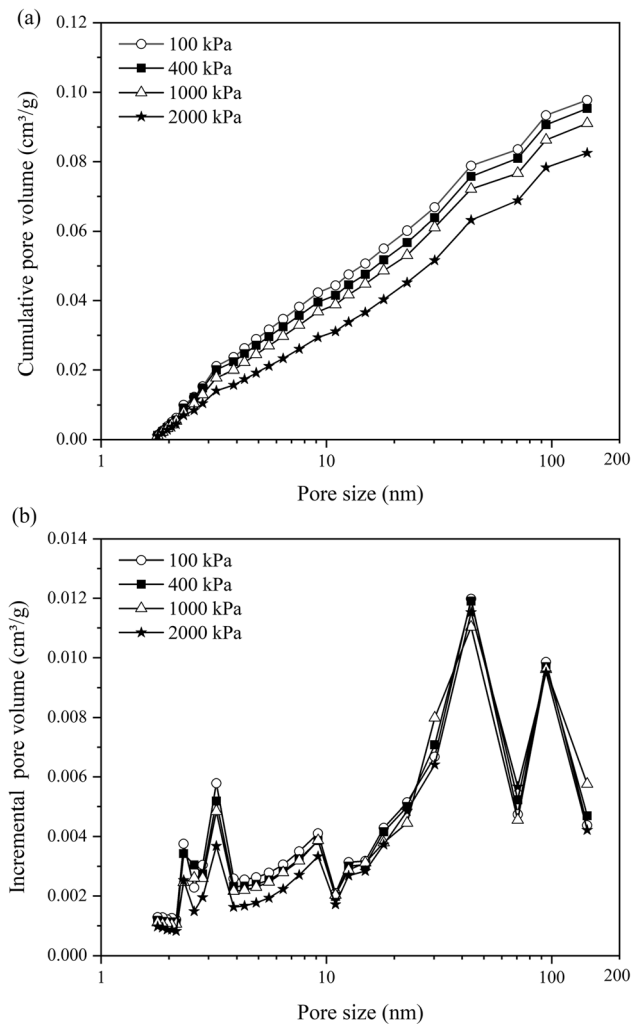

Fig. 8 Pore size distribution curves of the reconstituted illite-dominant clay samples at different vertical consolidation pressures determined by N$_2$GA technique in the range of 2–150 nm: **a** cumulative curves and **b** density function curves

Based on the MIP results, Zheng et al. [47] pointed out that during 1D compression, the macroscopic deformation of the reconstituted illite-dominant clay, which is identical to the soil used in this study, was mainly due to the collapse of the larger inter-aggregate pores. Combining the above analysis results with the findings of Zheng et al. [47], the porosity evolution of the illite-dominant clay during consolidation from nanometre scale to micron scale can be demonstrated, as shown in Fig. 9. Note that these schematic diagrams, showing clay layer, clay particle, clay aggregate, and the assembly of aggregates, is relatively simple, which is mainly used to distinguish between inter-layer, inter-particle, and inter-aggregate pores, while the actual microstructure of the illite-dominant clay is more complex.
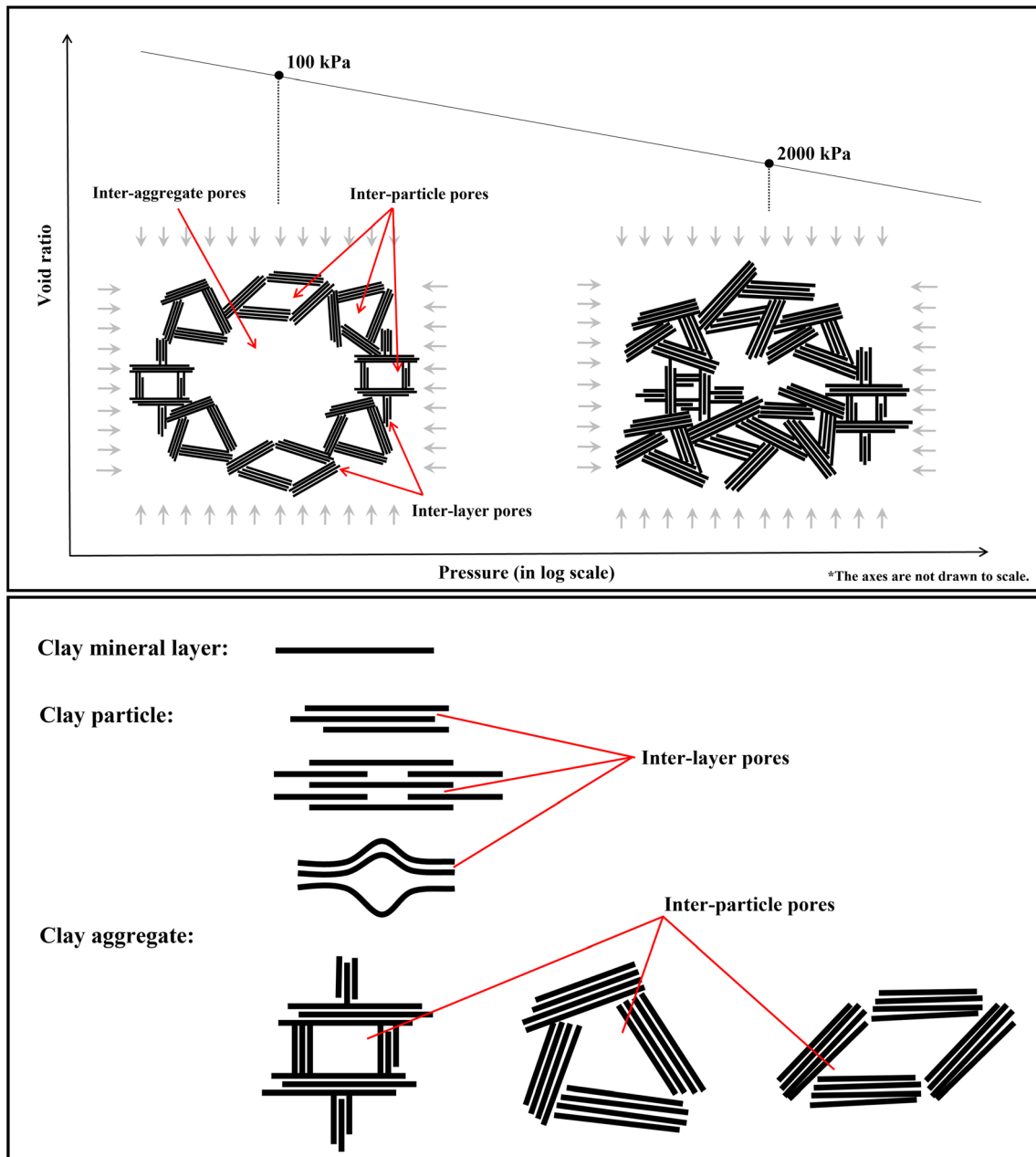
Fig. 9 Schematic diagram of the porosity evolution of illite-dominant clay during consolidation, note that the clay layer, clay particle, clay aggregate, and the assembly of aggregates in the diagram are relatively simple and schematic

4.4 Comparison of the pore-size distribution from MIP and N₂GA techniques

Since there is a common measurement range for pore size distribution (PSD) between the N₂GA and MIP techniques, i.e., 5–150 nm, the PSDs in this range covered by both techniques are compared, as shown in Fig. 10, where MIP data are reproduced from Zheng et al. [47]. Note again that the illitic clay in Zheng et al. [47] used for MIP testing is identical to the illite-dominant clay in the present study. The soil samples in this article were retrieved from the

specimens presented in Zheng et al. [47] which had been compressed one-dimensionally in an oedometer before preserving. From each tested specimen, at least five smaller cubic samples were freeze-dried, and these small soil sticks were then used for MIP testing, SEM investigation, N₂GA testing, TEM observations, and SAXS measurements. It can be seen that for this illite-dominant clay, there is an apparent mismatch in the shape of the PSDs obtained by N₂GA and MIP techniques (Fig. 10), which accords with the previous observations by Sills et al. [40] on washed goethite, Dullien and Dhawan [17] on sandstones, Kuila
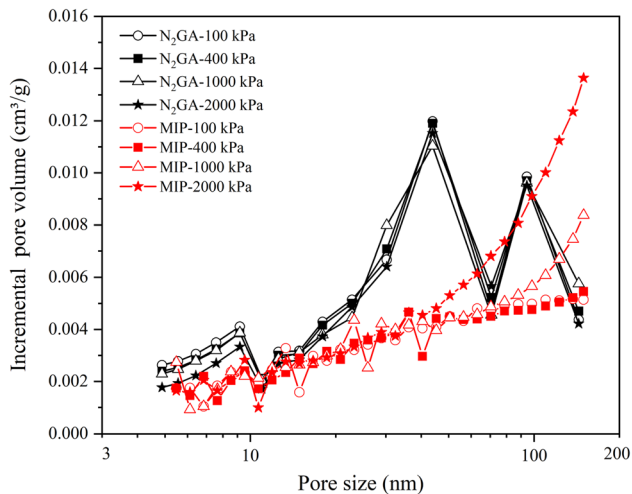
Fig. 10 Comparison of the PSDs in the common range of 5–150 nm determined by MIP and N₂GA techniques, where MIP data are reproduced from Zheng et al. [47]

and Prasad [25] on Wyoming montmorillonite, Kuila [24] on Georgia kaolinite, Li et al. [28] on Damintun Sag shale, and Zeng et al. [45] on magenta mudstone. In the existing literature, this discrepancy is often attributed to the different simplifying assumptions applied by the two methods. For example, in the N_2GA test, some models (such as the Density Functional Theory model) used to evaluate PSD are based on the assumption of slit-shaped pores rather than the cylindrical pores with a constant radius as employed in the MIP test [17, 40]. In addition, the contact mercury-solid angle is commonly assumed to be 140° in the MIP test, which may not be accurate [18, 25, 34]. Sills et al. [40] pointed out that using the commonly accepted contact angle of 140° for mercury, there was an approximately 20% shift between the PSDs obtained from N_2GA and MIP testing, but the PSD plots from both techniques could coincide by adjusting the contact angle from 140° to 153°. Kuila [24] also demonstrated that when using the BJH model to calculate PSD in the N_2GA test, several equations can be used to calculate the thickness of the adsorbed layer, but the difference in pore volume for each pore size obtained using different assumed thickness equations can vary by up to 60%. Other sources of the discrepancy also include that the high mercury intrusion pressure required to penetrate the smaller pores might break the skeletal pore structure and open some closed pores, and the specimens used for N_2GA testing need to be crushed, which may lead to some intra-aggregate pores being exposed [28, 45].

Although the BJH model with the assumption of cylindrical pores was used, the clay samples used for N_2GA testing were also not crushed, as well as the contact mercury-solid angle and the thickness equation for adsorbed

layer were selected appropriately based on the literature, the mismatch of the PSDs determined by the two methods can still be observed in Fig. 10. Based on this, a new explanation is proposed in this study for this discrepancy from the perspective of the liquid properties used by N_2GA and MIP techniques, which lead to different measuring mechanisms for interconnected pore space. Mercury is a typical non-wetting liquid, while liquid nitrogen is a wetting liquid with a contact angle smaller than 30° [6]. In the N_2GA measurement, the pore size distributions were determined based on the BJH model by using the adsorption isotherm that corresponds to a wetting path, while in MIP tests, the pore size distributions used for analysis were derived from the mercury intrusion curve corresponding to a drying process. Specifically, during the mercury intrusion process, mercury first fills the larger pores at lower pressure and then gradually fills smaller pores as the pressure increases. This drying process is affected by a bottle neck effect and is only able to measure the entrance diameter of pores. Similarly to the nitrogen desorption process, nitrogen in the largest pores is first emptied by capillary evaporation and then gradually drained out of the smaller pores. This drying process is controlled by the pore throats as well because if there is nitrogen left in the smaller pores, the larger pore connected by smaller pores cannot be emptied [10, 24]. On the other hand, during the nitrogen adsorption process, nitrogen is first adsorbed onto the surface of the smallest pore at the lowest relative pressure and then adsorbed successively on the surface of pores with the order from small to large. This wetting process of N_2GA provides a pore-body distribution instead of a pore-throat measurement from the drying process of MIP [25]. The essence of the difference in PSDs is therefore the sequential nature of the processes (drying and wetting processes). To make the pore size distributions obtained from both techniques comparable in the common region, it seems that one should combine the mercury intrusion with nitrogen desorption or combine the mercury extrusion with nitrogen adsorption.

5 Conclusions

The evolution of nano-pores, covering inter-layer pores and inter-particle pores, in an illite-dominant clay during consolidation was characterised and analysed quantitatively by using SAXS and N_2GA techniques. The following conclusions could be drawn:

1. By comparing the pore-size distribution curves of the oven-dried clay samples consolidated at different stress levels, it is found that the intra-aggregate pores (smaller than 100 nm in this study) are also affected

by 1D compression loading, at least in an illite-dominant soil, rather than remaining constant as previously thought in the literature.

2. Within the intra-aggregate pores, the inter-layer pores inside the clay particles stay unchanged with the increase of consolidation pressure, at least up to 4 MPa, which is confirmed by the SAXS test results showing no appearance of new peaks or the shifts of initial characteristic peaks in the 1D scattering intensity curves during consolidation. This provides the experimental basis for the general recognition in the literature that mechanical loading has little effect on the intra-particle structure of clay minerals.

3. Although compared to inter-aggregate pores, inter-particle pores make a small contribution to the macroscopic volume changes of the soil during consolidation, as the compression proceeds, the volume of inter-particle pores inside the aggregate does decrease by 0.015 cm^3/g, from 0.098 cm^3/g at 100 kPa to 0.083 cm^3/g at 2,000 kPa, which is probably due to the rearrangement of the particles composing the aggregates. This is accompanied by a gradual reduction in specific surface area of 4.09 m^2/g, from 55.47 m^2/g at 100 kPa to 51.38 m^2/g at 2000 kPa. The inter-particle pores are compressed as a whole during consolidation instead of the progressive collapse in an ordered manner, from the larger to the smaller.

4. Based on the existing research on the evolution of interaggregate pores during 1D loading, this study draws a more complete picture of the porosity evolution of the illite-dominant clay during consolidation, from nanometre scale to micron scale, contributing to the limited geotechnical database on microporosity.

5. For an illite-dominant clay, an apparent mismatch in the shape of the pore-size distributions is found in the common range covered by N_2GA and MIP techniques, which is consistent with observations on other materials with different clay mineralogy in the literature. In addition to some different simplifying assumptions applied by the two techniques contributing to the discrepancy, a new explanation is proposed from the perspective of the liquid properties used by N_2GA and MIP techniques, corresponding to the sequential nature of the drying and wetting processes, a point which is usually ignored.

6. The nitrogen gas adsorption technique and small angle X-ray scattering measurement used in conjunction with each other appear as a promising approach for clay nano-pores identification, providing supplementary information that is not typically available if using only MIP technology.

Data availability The data sets generated during and/or analysed during the current study are available from the corresponding author on reasonable request.

Declarations

Conflict of interest The authors declare that they have no known competing financial interests or personal relationships that could have appeared to influence the work reported in this paper.

References

1. Barrett EP, Joyner LG, Halenda PP (1951) The determination of pore volume and area distributions in porous substances. I. Computations from nitrogen isotherms. J Am Chem Soc 73(1):373–380

2. Bayliss P (1989) Unit-cell dimensions of two-dimensionai clay minerals. Powder Diffr 4(1):19–20

3. Bennett RH, Hulber MH (1986) Clay microstructure. International Human Resources Development Corporation Press, Prentice Hall, Boston, p 161

4. Bertagnolli C, Kleinübing SJ, Da Silva MGC (2011) Preparation and characterization of a Brazilian bentonite clay for removal of copper in porous beds. Appl Clay Sci 53(1):73–79

5. Birmpilis G, Hall SA, Lages S, Dijkstra J (2019) Monitoring of the nano-structure response of natural clay under mechanical perturbation using small angle X-ray scattering and digital image correlation. Acta Geotech 14(6):1965–1975

6. Brennan PJ, Skrabek EA (1971) Design and development of a prototype static cryogenic heat transfer system. NASA CR-121939

7. Burland JB (1990) On the compressibility and shear strength of natural clays. Géotechnique 40(3):329–378

8. Brown G (1982) Crystal structures of clay minerals and their X-ray identification (Vol. 5). The Mineralogical Society of Great Britain and Ireland

9. Brunauer S, Emmett PH, Teller E (1938) Adsorption of gases in multimolecular layers. J Am Chem Soc 60(2):309–319

10. Conner WC, Cevallos-Candau JF, Weist EL, Pajares J, Mendioroz S, Cortes A (1986) Characterization of pore structure: porosimetry and sorption. Langmuir 2(2):151–154

11. Clarkson CR, Solano N, Bustin RM, Bustin AMM, Chalmers GR, He L, Melnichenko YB, Radliński AP, Blach TP (2013) Pore structure characterization of North American shale gas reservoirs using USANS/SANS, gas adsorption, and mercury intrusion. Fuel 103:606–616

12. Delage P, Pellerin FM (1984) Influence de la lyophilisation sur la structure d'une argile sensible du Québec. Clay Miner 19(2):151–160

13. Delage P, Lefebvre G (1984) Study of the structure of a sensitive Champlain clay and of its evolution during consolidation. Can Geotech J 21(1):21–35

14. Delage P, Marcial D, Cui YJ, Ruiz X (2006) Ageing effects in a compacted bentonite: a microstructure approach. Géotechnique 56(5):291–304

15. Delage P, Tessier D (2021) Macroscopic effects of nano and microscopic phenomena in clayey soils and clay rocks. Geomech Energy Environ 27:100177

16. Diamond S (1970) Pore size distributions in clays. Clays Clay Miner 18(1):7–23

17. Dullien FAL, Dhawan GK (1974) Characterization of pore structure by a combination of quantitative photomicrography and mercury porosimetry. J Colloid Interface Sci 47(2):337–349

18. Gregg SJ, Sing KSW (1982) Adsorption, surface area and porosity. Academic Press, London

19. Griffiths FJ, Joshi RC (1989) Change in pore size distribution due to consolidation of clays. Géotechnique 39(1):159–167

20. Guinier A, Fournet G, Yudowitch KL (1955) Small-angle scattering of X-rays. Wiley, New York

21. Guglielmi S (2018) Evolution of the clay micro-structure in compression and shearing loading paths (Doctoral dissertation, PhD thesis, Polytechnic University of Bari).

22. Guglielmi S, Cotecchia F, Cafaro F, Gens A (2022) Analysis of the micro to macro response of clays to compression. Géotechnique. https://doi.org/10.1680/jgeot.21.00233

23. Hegyesi N, Vad RT, Pukánszky B (2017) Determination of the specific surface area of layered silicates by methylene blue adsorption: the role of structure, pH and layer charge. Appl Clay Sci 146:50–55

24. Kuila U (2013) Measurement and interpretation of porosity and pore-size distribution in mudrocks: the hole story of shales. Colorado School of Mines

25. Kuila U, Prasad M (2013) Specific surface area and pore-size distribution in clays and shales. Geophys Prospect 61:341–362

26. Laity PR, Asare-Addo K, Sweeney F, Šupuk E, Conway BR (2015) Using small-angle X-ray scattering to investigate the compaction behaviour of a granulated clay. Appl Clay Sci 108:149–164

27. Lastoskie C, Gubbins KE, Quirke N (1993) Pore size distribution analysis of microporous carbons: a density functional theory approach. J Phys Chem 97(18):4786–4796

28. Li J, Yin J, Zhang Y, Lu S, Wang W, Li J, Chen F, Meng Y (2015) A comparison of experimental methods for describing shale pore features: a case study in the Bohai Bay Basin of eastern China. Int J Coal Geol 152:39–49

29. Mitchell JK, Soga K (2005) Fundamentals of soil behavior, vol 3. Wiley, New York

30. Morvan M, Espinat D, Lambard J, Zemb T (1994) Ultrasmall-and small-angle X-ray scattering of smectite clay suspensions. Colloids Surf A 82(2):193–203

31. Neimark AV, Lin Y, Ravikovitch PI, Thommes M (2009) Quenched solid density functional theory and pore size analysis of micro-mesoporous carbons. Carbon 47(7):1617–1628

32. Ninjgarav E, Chung SG, Jang WY, Ryu CK (2007) Pore size distribution of Pusan clay measured by mercury intrusion porosimetry. KSCE J Civ Eng 11(3):133–139

33. Nowamooz H, Masrouri F (2010) Influence of suction cycles on the soil fabric of compacted swelling soil. CR Geosci 342(12):901–910

34. Penumadu D, Dean J (2000) Compressibility effect in evaluating the pore-size distribution of kaolin clay using mercury intrusion porosimetry. Can Geotech J 37(2):393–405

35. Reatto A, Bruand A, Silva EM, Guégan R, Cousin I, Brossard M, Martins ES (2009) Shrinkage of microaggregates in Brazilian Latosols during drying: significance of the clay content, mineralogy and hydric stress history. Eur J Soil Sci 60(6):1106–1116

36. Reed MA, Lovell CW, Altschaeffl AG, Wood LE (1980) Frost-heaving rate predicted from pore-size distribution: reply. Can Geotech J 17(4):639–640

37. Rocchi I, Coop MR (2014) Experimental accuracy of the initial specific volume. Geotech Test J 37(1):169–175

38. Santamarina JC, Klein KA, Wang YH, Prencke E (2002) Specific surface: determination and relevance. Can Geotech J 39(1):233–241

39. Sing KS (1985) Reporting physisorption data for gas/solid systems with special reference to the determination of surface area and porosity (Recommendations 1984). Pure Appl Chem 57(4):603–619

40. Sills ID, Aylmore LAG, Quirk JP (1973) A comparison between mercury injection and nitrogen sorption as methods of determining pore size distributions. Soil Sci Soc Am J 37(4):535–537

41. Skempton AW, Sowa VA (1963) The behaviour of saturated clays during sampling and testing. Geotechnique 13(4):269–290

42. Tanaka H, Shiwakoti DR, Omukai N, Rito F, Locat J, Tanaka M (2003) Pore size distribution of clayey soils measured by mercury intrusion porosimetry and its relation to hydraulic conductivity. Soils Found 43(6):63–73

43. Thompson ML, McBride JF, Horton R (1985) Effects of drying treatments on porosity of soil materials. Soil Sci Soc Am J 49(6):1360–1364

44. Yu CY, Chow JK, Wang YH (2016) Pore-size changes and responses of kaolinite with different structures subject to consolidation and shearing. Eng Geol 202:122–131

45. Zeng Z, Kong L, Wang M, Wang J (2020) Effects of remoulding and wetting-drying-freezing-thawing cycles on the pore structures of Yanji mudstones. Cold Reg Sci Technol 174:103037

46. Zhang S, Liu Q, Cheng H, Li X, Zeng F, Frost RL (2014) Intercalation of dodecylamine into kaolinite and its layering structure investigated by molecular dynamics simulation. J Colloid Interface Sci 430:345–350

47. Zheng Y, Baudet BA, Delage P, Pereira JM, Sammonds P (2022) Pore changes in an illitic clay during one-dimensional compression. Géotechnique. https://doi.org/10.1680/jgeot.21.00206